Hindawi
Journal of Mathematics
Volume 2022, Article ID 4977793, 15 pages
https://doi.org/10.1155/2022/4977793

Research Article

Investigation of Relaxation Time on Viscoelastic Two-Dimensional Flow Characteristics Using FreeFem++

Muhammad Sabeel Khan,[1] **M. Asif Memon**,[1,2] **and Ebenezer Bonyah**[3]

[1]*Department of Mathematics and Social Sciences, Sukkur IBA University, Sukkur 65200, Sindh, Pakistan*
[2]*Department of Mathematics, Universiti Tun Hussein Onn Malaysia (UTHM), 86400 Parit Raja, Batu Pahat, Johor, Malaysia*
[3]*Department of Mathematics Education, Akenten Appiah Menka University of Skills Training and Entrepreneurial, Kumasi, Ghana*

Correspondence should be addressed to Ebenezer Bonyah; ebonyah@aamusted.edu.gh

Received 15 January 2022; Accepted 26 May 2022; Published 21 June 2022

Academic Editor: Melike Kaplan

Viscoelastic fluid flow models have shown promising scope in modeling the behavior of many industrial materials such as polymeric materials, microfluidics, biological liquids, gels, plastic melts, and geomaterials. The relaxation time in these models is of great physical significance. In this article, we study the impact of relaxation time on the viscoelastic flow characteristics in a two-dimensional baffled cavity. To the best of authors' knowledge, relaxation time impact on the chosen flow characteristics in the present context has not been studied and presented in the literature before. The constitutive theory of upper convected Maxwell viscoelastic flow incorporating the viscosity ad relaxation time is taken into consideration. To this account, the flow governing PDEs are derived, and an unsteady variational numerical approach based on classical variational setting is presented. A numerical algorithm based on characteristic Galerkin finite elements method is designed and implemented using the programming language FreeFem++. Computations are carried out and drag and lift forces along with other parameters of interests are calculated. Impact of relaxation time on these flow characteristics are studied and analyzed. The relaxation time R_f is assumed to be in the range of $0 \leq R_f \leq 1 \times 10 - 3$. The flow simulations are carried out for large Reynolds number in the range of $200 \leq \mathrm{Re} \leq 5000$. In addition to the application of FreeFem++, some new and interesting features of the flow characteristics are presented and discussed.

1. Introduction

In nature complex fluids such as viscoelastic or microfluidic mixtures surround many important phenomena, and therefore, investigation of such fluids can play an important role in the development of many industrial processes. These industrial processes range from polymeric melting processes [1, 2], pulp fibers [3, 4], mineral processing [5], food processing [6]; and references therein, cement pastes and cosmetics processing [7]; and reference therein, and biophysical processes [8–10]. Also, viscoelastic flows are seen to be generated in simple liquids by the vibration of nanostructures, see for instance [8], and references present therein.

Viscoelastic behavior of flows has been studied in the literature so far in varying contexts. For instance, Boyang in his PhD dissertation [11] investigated the flow of polymeric viscoelastic fluid in three different geometries where it was observed that fluid relaxation influences the onset of turbulence in shear flows. For a review and state of the art on the effect of viscoelastic fluid flows and their applications, a/ the reader is referred to the work of Yuan et al. [12]. For a review and state-of-the-art research on viscoelastic fluids in particle focusing and related particle manipulation applications, the reader is referred to the work of Chen [9]. Swimming of ciliated cells in a viscoelastic Giesekus fluid is investigated in the work of Zhu et al. [13]. They observe a decay in the flow velocity of the fluid in the presence of polymeric stresses. The main characteristic of their investigation was the behavior of the Weissenberg number on the polymeric swimmers using numerical simulation through the finite element method. Having applications in health and diseases, see for instance the review article by Sebastian and

Dittrich [14], the microfluidics which are viscoelastic in nature are used to mimic the blood flow in the/a human body. Also, viscoelastic transport of the female sperm is evidenced in the work of Suarez and Pacey [15]. To understand the practical application of viscoelastic fluids in porous media, the reader is referred to the work of Haward et al. [16]. The kinematics of DNA flows is quantified with the application of viscoelastic microflows in the work of Gulati et al. [17]. On the practical problems involving viscoelastic behaviour in biological dynamics, the review article by Goldstein [18] is referred to the reader. In connection to the clinical experimentation and microfluidics to study the behaviour of neutrophil genomics and proteomics, the reader is referred to the work of Kotz et al. [19]. Liu et al. [20] used viscoelastic fluids to study the separation of *Bacillus* population in microfluidics.

The flow of these complex fluids is resolved by using a number of numerical algorithms in the literature; in this regard, the reader is referred to a comprehensive review article of Alves et al. [21] on the numerical methods for viscoelastic fluid flows.

Although many important applications [1–10] are realizing the investigation of viscoelastic flows, the effect of fluid relaxation time in these models has been rarely investigated. Among the existing literature only few studies are dealing with the study of fluid relaxation time but in different contexts. For instance, Mahapatra and Bandopadhyaya [22] observed the effect of fluid relaxation time and retardation time over a nonuniformly charged surface in the electroosmosis of a viscoelastic fluid. In an annular domain, Dey [23] observed that the fluid relaxation time affects the hydromagnetic viscoelastic flow maximum at the center portion of the geometry. Eldesoky [24] analyzed various effects of relaxation time in a compressible Maxwellian peristaltic slip flow, but in one-dimensional settings. The influence of relaxation time on the locomotion of the microorganisms is analyzed by Josef [25] where it was observed that the fluid relaxation time can increase the speed and thus the efficiency of a swimmer swimming freely in a viscoelastic fluid medium. Looking towards the importance and applications of viscoelastic fluids, it is therefore believed that to understand the behavior of complex fluids and microfluidic mixtures having viscoelastic like structure, the study of relaxation time needs further attention.

The aim of this article is to present an investigation of fluid relaxation time on the evolution of viscoelastic flow dynamics where different parameters of study are taken into consideration. The governing flow equations are modeled, and the variational framework based on the characteristic Galerkin method is developed and implemented using FreeFem++ [26]. Numerical simulations are performed, and some important features of the flow dynamics are observed and discussed. The rest of the paper is organized as follows: The flow governing equations of viscoelastic fluid are introduced in Section 2, and a time relaxation mathematical model is presented. In Section 3, classical variational formulation of the flow governing equations is constructed. In Section 4, numerical simulations are shown, and results are presented and discussed. Finally, conclusions are drawn in section 5.

2. Viscoelastic Relaxation-Time Mathematical Model

One of the widely appreciated models to describe the viscoelastic fluids is the upper convected Maxwell (UCM) model that incorporates viscosity and relaxation time with the following constitutive equation:

$$\lambda_{\tau}^{\nabla} + \tau = -2\eta \mathbf{d}(\mathbf{v}), \tag{1}$$

where λ and η are the fluid characteristic relaxation time and the fluid viscosity, respectively. The deformation strain tensor $\mathbf{d}(\mathbf{v})$ in (1) is defined as

$$\mathbf{d}(\mathbf{V}) = \frac{1}{2}\left(\nabla v + (\nabla v)^T\right). \tag{2}$$

$\overset{\nabla}{\tau}$ being the upper convected derivative is defined as

$$\overset{\nabla}{\tau} = \frac{\partial \tau}{\partial t} + v.\nabla\tau - (\nabla v).\tau - \tau.(\nabla v)^T. \tag{3}$$

Here, λ and η are assumed to be constant, whereas in general, they may depend on the local shear rate, pressure, and temperature, see for instance [21]. After following [27], the governing equation of motion for the unsteady incompressible flow is stated as

$$\rho\left(\frac{\partial v}{\partial t} + v.\nabla v\right) + \nabla p + \nabla.\tau = b, \tag{4}$$

together with the mass conservation within the medium

$$\nabla.v = 0. \tag{5}$$

Consider a two-dimensional unsteady incompressible viscoelastic flow confined in a lid-driven baffled cavity as depicted in Figure 1. In the absence of body forces b, the momentum balance and continuity equations in (4) and (5) read in the component form as

$$\frac{\partial u}{\partial x} + \frac{\partial u}{\partial y} = 0, \tag{6}$$

$$\frac{\partial u}{\partial t} + u\frac{\partial u}{\partial x} + v\frac{\partial u}{\partial y} + \lambda\left(u^2\frac{\partial^2 u}{\partial x^2} + v^2\frac{\partial^2 u}{\partial y^2} + 2uv\frac{\partial^2 u}{\partial x \partial y}\right) = -\frac{1}{\rho}\frac{\partial p}{\partial x} + \nu\left(\frac{\partial^2 u}{\partial x^2} + \frac{\partial^2 u}{\partial y^2}\right), \tag{7}$$

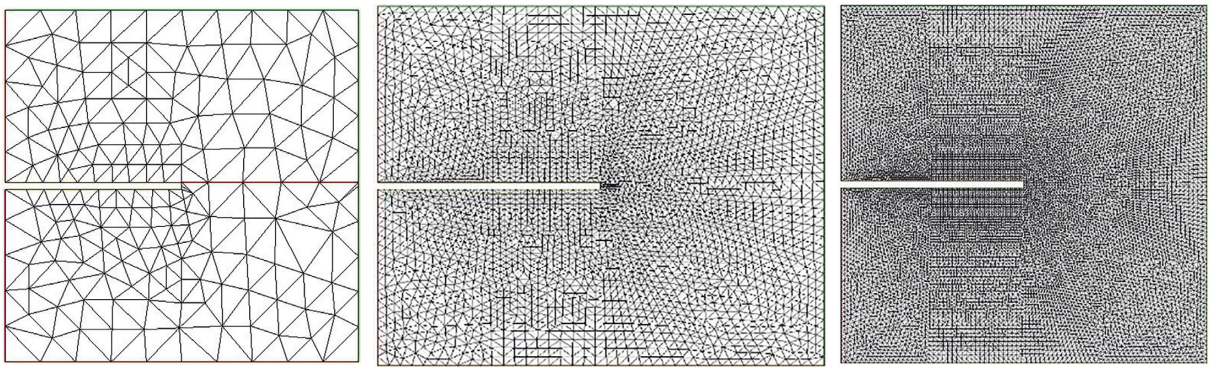

Figure 1: Computational meshes (from left to right): coarser, refined, and finer.

$$\frac{\partial v}{\partial t} + u\frac{\partial v}{\partial x} + v\frac{\partial v}{\partial y} + \lambda\left(u^2\frac{\partial^2 v}{\partial x^2} + v^2\frac{\partial^2 v}{\partial y^2} + 2uv\frac{\partial^2 v}{\partial x \partial y}\right) = -\frac{1}{\rho}\frac{\partial p}{\partial y} + \nu\left(\frac{\partial^2 v}{\partial x^2} + \frac{\partial^2 v}{\partial y^2}\right). \tag{8}$$

Let us introduce the following transformations to obtain the dimensionless forms of the set of PDEs in (7) and (8)

$$\begin{aligned} U &= \frac{u}{u_0}, \\ V &= \frac{v}{v_0}, \\ T &= \frac{tL}{u_0}, \\ X &= \frac{x}{L}, \\ Y &= \frac{y}{L}, \\ P &= \frac{p}{\rho u_0^2}, \end{aligned} \tag{9}$$

where L is the width of the cavity. The dimensionless forms of the x-momentum in equation (7) and y momentum in (8) along with the continuity equation thus read as

$$\frac{\partial U}{\partial X} + \frac{\partial U}{\partial Y} = 0, \tag{10}$$

$$\frac{\partial U}{\partial T} + U\frac{\partial U}{\partial X} + V\frac{\partial U}{\partial Y} + R_f\left(U^2\frac{\partial^2 U}{\partial X^2} + V^2\frac{\partial^2 U}{\partial Y^2} + 2UV\frac{\partial^2 U}{\partial X \partial Y}\right) = -\frac{\partial P}{\partial X} + \frac{1}{R_e}\left(\frac{\partial^2 U}{\partial X^2} + \frac{\partial^2 U}{\partial Y^2}\right), \tag{11}$$

$$\frac{\partial V}{\partial T} + U\frac{\partial V}{\partial X} + V\frac{\partial V}{\partial Y} + R_f\left(U^2\frac{\partial^2 V}{\partial X^2} + V^2\frac{\partial^2 V}{\partial Y^2} + 2UV\frac{\partial^2 V}{\partial X \partial Y}\right) = -\frac{\partial P}{\partial X} + \frac{1}{R_e}\left(\frac{\partial^2 V}{\partial X^2} + \frac{\partial^2 V}{\partial Y^2}\right). \tag{12}$$

In (11) and (12), the nondimensional parameters R_e represent Reynolds number, and R_f is the fluid relaxation time, respectively, defined by

$$\begin{aligned} R_e &= \frac{\rho L u_0}{\mu}, \\ R_e &= \frac{\lambda u_0}{L}. \end{aligned} \tag{13}$$

3. Numerical Strategy and Classical Weak Formulation

In order to solve the above strong form of the PDEs in (10)–(12), we use the finite element method where the weak formulation of the time discretized model is presented in this section. Let us discretize the time domain by a time step length $\Delta t > 0$ in n subintervals with $t_n = n\Delta t$. To obtain a time discretized variational formulation, we use the method of characteristics whereby defining the characteristic trajectory at any time t through $\mathbf{x}$ as

$$\frac{\partial \mathbf{X}}{\partial \tau}(x,t,\tau) = v(\mathbf{X}(x,t,\tau),\tau), \tag{14}$$

where $\mathbf{X}|_{\tau=t} = x$.

We define the total derivative by assuming a function $\phi(\mathbf{x},t)$ by

$$\frac{D}{Dt}(x,t) = \left(\frac{\partial \phi}{\partial t} + v.\nabla\phi\right)(x,t) = \frac{\partial}{\partial t}(\phi(\mathbf{X}(x,t,\tau),\tau))|_{\tau=t}. \tag{15}$$

Now, since $x = \mathbf{X}(x, t_{n+1}, t_{n+1})\ \boldsymbol{x}$, it is therefore the total derivative of ϕ becomes

$$\left(\frac{D\phi}{Dt}\right)^{n+1}(x) \approx \frac{\phi^{n+1}(x) - \phi^n(\mathbf{X}^n(x))}{\Delta t}, \tag{16}$$

where $\mathbf{X^n}(x)$ approximates the $\mathbf{X}(x, t_{n+1}, t_{n+1})$. For detail description of this method, the reader is referred to the work by Pironneau and Tezduyar [28]. Define the functional space $\sum_\Omega = \{v \in H_0^1(\Omega), \nabla.v = 0\}$ as space of divergence-free functions. The time incremental variational formulation thus reads.

Given $\{U^n, V^n\}$ and P^n at time step t_n find $\{U^{n+1}, V^{n+1}\} \in H_0^1(\Omega)$ and $P^{n+1} \in L^2(\Omega)$ at time step t_{n+1}, such that

$$\begin{aligned}
&\frac{1}{\delta t}\int_\Omega U^{n+1}\widehat{U}d\Omega + \int_\Omega\left\{\frac{\partial P^{n+1}}{\partial X^{n+1}}\widehat{U} + \frac{1}{R_e}\left(\frac{\partial U^{n+1}}{\partial X^{n+1}}\frac{\partial \widehat{U}}{\partial X^{n+1}} + \frac{\partial U^{n+1}}{\partial Y^{n+1}}\frac{\partial \widehat{U}}{\partial Y^{n+1}}\right)\right\}\mathrm{d}\Omega \\
&= \frac{1}{\delta t}\int_\Omega (U^n o\, X^n)\widehat{U}d\Omega + R_f\int_\Omega\left\{2U^{n+1}\left(\frac{\partial U^{n+1}}{\partial X^{n+1}} + \frac{\partial V^{n+1}}{\partial Y^{n+1}}\right)\frac{\partial U^{n+1}}{\partial X^{n+1}}\widehat{U} + U^{2n+2}\frac{\partial U^{n+1}}{\partial X^{n+1}}\frac{\partial \widehat{U}}{\partial X^{n+1}}\right. \\
&\left. + 2V^{n+1}\left(\frac{\partial V^{n+1}}{\partial Y^{n+1}} + \frac{\partial U^{n+1}}{\partial X^{n+1}}\right)\frac{\partial U^{n+1}}{\partial Y^{n+1}}\widehat{U} + V^{2n+2}\frac{\partial U^{n+1}}{\partial Y^{n+1}}\frac{\partial \widehat{U}}{\partial Y^{n+1}} + 2U^{n+1}V^{n+1}\frac{\partial U^{n+1}}{\partial Y^{n+1}}\frac{\partial \widehat{U}}{\partial X^{n+1}}\right\}\mathrm{d}\Omega,
\end{aligned} \tag{17}$$

$$\begin{aligned}
&\frac{1}{\delta t}\int_\Omega V^{n+1}\widehat{V}d\Omega + \int_\Omega\left\{\frac{\partial P^{n+1}}{\partial Y^{n+1}}\widehat{V} + \frac{1}{R_e}\left(\frac{\partial V^{n+1}}{\partial X^{n+1}}\frac{\partial \widehat{V}}{\partial X^{n+1}} + \frac{\partial V^{n+1}}{\partial Y^{n+1}}\frac{\partial \widehat{V}}{\partial Y^{n+1}}\right)\right\}\mathrm{d}\Omega \\
&= \frac{1}{\delta t}\int_\Omega (V^n o\, Y^n)\widehat{V}d\Omega + R_f\int_\Omega\left\{2U^{n+1}\left(\frac{\partial U^{n+1}}{\partial X^{n+1}} + \frac{\partial V^{n+1}}{\partial Y^{n+1}}\right)\frac{\partial V^{n+1}}{\partial X^{n+1}}\widehat{V} + U^{2n+2}\frac{\partial V^{n+1}}{\partial Y^{n+1}}\frac{\partial \widehat{V}}{\partial Y^{n+1}}\right. \\
&\left. + 2V^{n+1}\left(\frac{\partial V^{n+1}}{\partial Y^{n+1}} + \frac{\partial U^{n+1}}{\partial X^{n+1}}\right)\frac{\partial V^{n+1}}{\partial Y^{n+1}}\widehat{V} + V^{2n+2}\frac{\partial V^{n+1}}{\partial Y^{n+1}}\frac{\partial \widehat{V}}{\partial Y^{n+1}} + 2U^{n+1}V^{n+1}\frac{\partial V^{n+1}}{\partial Y^{n+1}}\frac{\partial \widehat{V}}{\partial X^{n+1}}\right\}\mathrm{d}\Omega,
\end{aligned} \tag{18}$$

subjected to the following boundary and initial conditions

$$\begin{aligned}
U^{n+1}(x,y) = 0, \forall (x,y) \in \partial\Omega(x, y = 0.5); \\
-0.5 \le x \le 0.5;\ \text{and}\ -0.5 \le y \le 0.5,
\end{aligned} \tag{19}$$

$$\begin{aligned}
V^{n+1}(x,y) = 0, \\
\forall (x,y) \in \partial\Omega,
\end{aligned} \tag{20}$$

$$\begin{aligned}
U^n(t = n\Delta t, x, y = 0.5) = 1.0; \quad (x, y = 0.5), \\
-0.5 \le x \le 0.5.
\end{aligned} \tag{21}$$

4. Numerical Results and Discussion

The set of governing (17) and (18) along with the associated boundary and initial conditions in (19), (20), and (21) are implemented through FreeFem++ [26]. The numerical results presented and tests are carried out with Reynolds number Re ranging between $200 \le \mathrm{Re} \le 5000$. The relaxation time R_f is assumed to be in the range of $0 \le R_f \le 1 \times 10^{-3}$. These numerical values for the relaxation times are taken phenomenological. However, exact values can be calculated by using the novel device [29] which is capable of measuring relaxation times of complex fluids. The parameters of

interests in these simulations are the drag force F_d, mass flow rate M_{flowrate}, maximum and minimum stream function values $\psi_{\max}$ and $\psi_{\min}$, respectively. Among the other parameters are the kinetic energy and flow field velocities. The finite element meshes in Figure 1 are used in these simulations. The mesh on the left is having 730 elements, 397 vertices, and 1523 number of degrees of freedom. The mesh in middle is having 5746 number of triangular elements, 2965 number of vertices, and 11675 number of degrees of freedom. The mesh on the right is having 10078 number of triangular elements, 5161 number of triangular elements, and 20399 number of degrees of freedom. In Figure 2, the stream function is plotted. In Figure 3, velocity magnitudes are shown for the varying value of fluid relaxation times in the case of Re = 5000. In the right-sided figure, a relaxation time $R_f = 1 \times 10^{-4}$, whereas in the left, $R_f = 0$ is used for the simulations. In Figure 4, the time evolution of mass flow rates for different simulations cases is shown. Four different test cases with Re = 500, 1000, 2000, and 5000 are computed, and the graphs of mass flow rates are calculated for varying values of fluid relaxation time. It is noted that the mass flow rates get fluctuations in time and reaches to a steady state after longer time evolve in the case of large Reynolds numbers as compared to small Reynolds numbers. It is also observed that the mass flow rate is increasing when the $\text{Re} \leq 1000$ and decreasing when $Re \geq 2000$ by increasing the fluid relaxation time R_f. This shows that in laminar regime of flow, the relaxation time aids the mass flow rate to rise, whereas in the transitional flow regime, relaxation time drops the mass flow rate.

In Figure 5, the time evolution of drag forces for different Reynolds numbers are shown with varying values of the relaxation time. It can be seen that the drag force fluctuates in time once the flow enters in the transitional regime, whereas in the laminar regime, the drag force fluctuations are not observed. Moreover, higher the Reynolds numbers in the transitional regime, larger are the fluctuations in the drag at the bottom surface of the cavity. The drag force at the bottom surface decreases as the relaxation time is increased in both the laminar and transitional regimes. The drag force is influenced by the particle velocities at the bottom surface as the moving particle near the bottom surface observes resistance in motion with the increasing value of the fluid relaxation time; therefore, the drag force is decreased as the fluid relaxation time is increased. In Figure 6, the drag forces are computed at the lid surface and are graphically presented over time for varying values of the Reynolds numbers Re and relaxation time R_f; it is observed that the drag force gets fluctuations in the transitional regime, whereas in the laminar regime of the flow, these fluctuations are not present. Also, these fluctuations in the drag force disappear and become negligibly small once the time is evolved, and the flow gets developed. The drag force has a nonmonotone behavior in the regime of small Reynolds numbers at the lid surface and decrease by increasing the relaxation time when the flow gets near the transitional regime. Once it enters the transitional regime, then the drag force get increased by increasing the relaxation time. This behavior of the drag force is due to the eddies produced in the regime of high Reynolds numbers which affect the evolution of the drag force at the lid of the cavity. In Tables 1 and 2, the horizontal and vertical velocities along the width and height of the cavity are studied with varying values of the relaxation time. The horizontal velocities near the top lid and near the bottom of the cavity increase in both the test cases by increasing the fluid relaxation time. It is observed that by increasing the relaxation time, the horizontal velocities are increasing over a larger depth of the cavity from the top lid in case of small Reynolds number as compared to the case of large Reynolds number whereas these flow velocities are increasing over a larger depth upward from the bottom surface of the cavity in case of large Reynolds number as compared to small Reynolds number by increasing the fluid relaxation time. However, in case of the small Reynolds number, the vertical velocities decrease by increasing the relaxation time, and this decrease in velocities is observed over a larger depth from the right end boundary of the cavity as compared to the case of the large Reynolds number.

Nevertheless, in case of large Reynolds number, vertical velocities attain increasing trend over a larger depth from the left end boundary of the cavity as compared to the case of small Reynolds number.

In Table 3, the kinetic energies are calculated in different presented test cases for varying values of the relaxation time R_f. It is observed that for increasing value of relaxation time, the kinetic energies of the system of particles are increasing. This shows that the relaxation time influences the magnitude of the fluid velocities of the system particles in the flow, and the translational motions of the particles get increased by increasing the fluid relaxation time. In Table 4, different parameters of interests are computed and presented for two different test cases, i.e., for Re = 200 and Re = 1000, with varying values of the relaxation time R_f. It can be observed that the minimum stream value $\psi_{\min}$ decreases with an increasing value of the relaxation time. The maximum stream value ψ_{max} increases with increasing relaxation time monotonically in the case of Re = 200, whereas this relation is nonmonotone in the case of Re = 1000. The maximum value of ψ_{max} for chosen relaxation times in the case of Re = 1000 is corresponding to $R_f = 2.0x10^{-3}$. The mass flow rate is increased by increasing the relaxation time. The drag force at the lid is increased by increasing relaxation time in the case of Re = 200, whereas in the case of $R = 1000$, a nonmonotone behavior is observed. This behavior of nonmonotonicity in the case of large Reynolds numbers is due to vortex nature of the flow field. In conjunction to this, the drag force at the bottom of the cavity surface is increasing for both the test cases by increasing the relaxation times. Based on the minimum values of the flow field velocities u and v, it can be observed that these velocities are increasing and decreasing, respectively, by increasing the relaxation time. However, the maximum values of the vertical velocity are increasing for both the test cases by increasing the value of relaxation time.

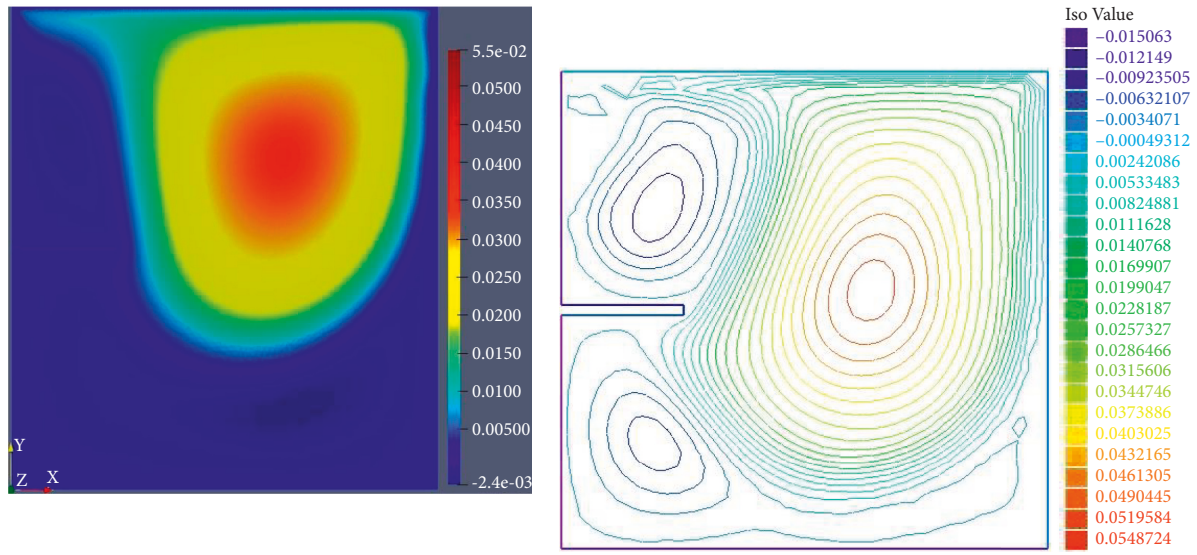

(a) (b)

Figure 2: Stream velocity plot (a) and iso-lines of velocity magnitude (b) at two different time iteration levels.

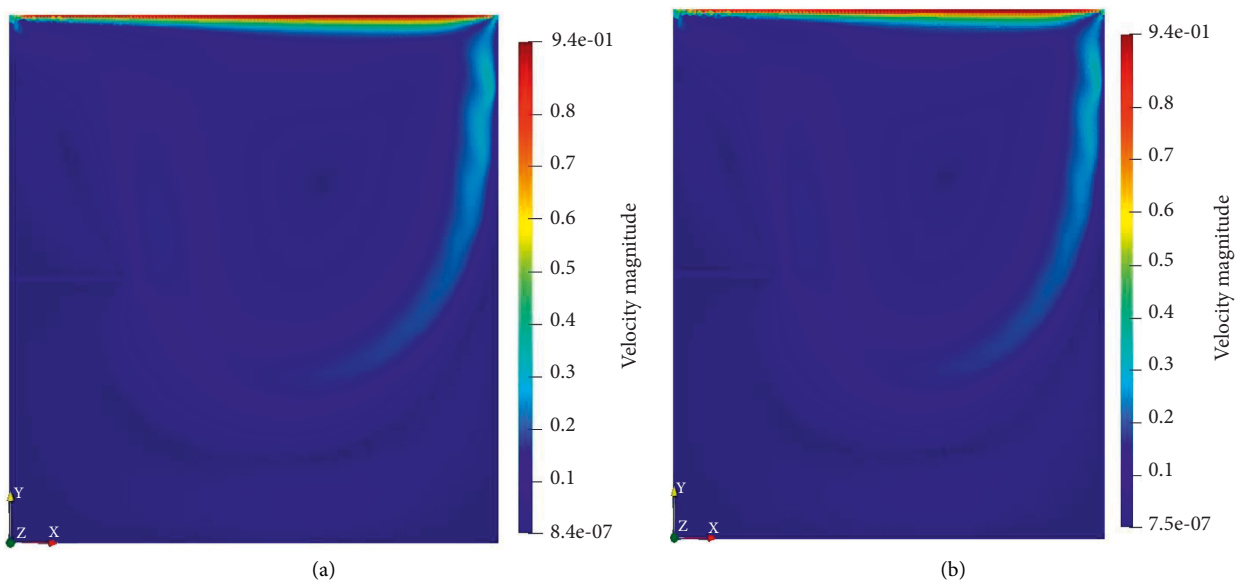

(a) (b)

Figure 3: Velocity magnitudes in case of Re = 5000 and for $Rf = 0$ (a), $Rf = 1 \times 10^{-4}$ (b).

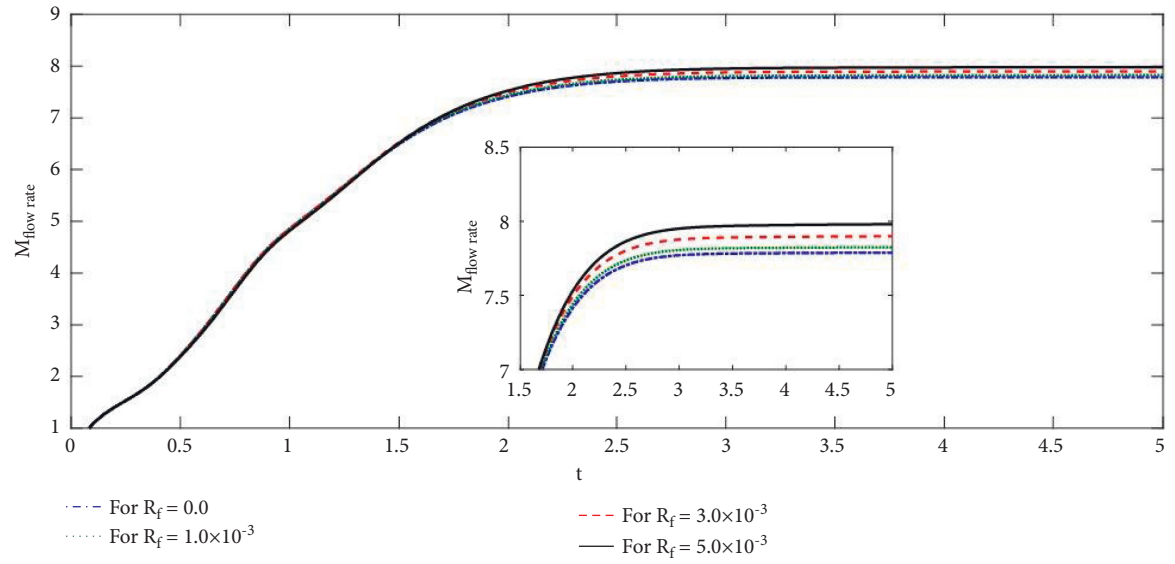

(a)

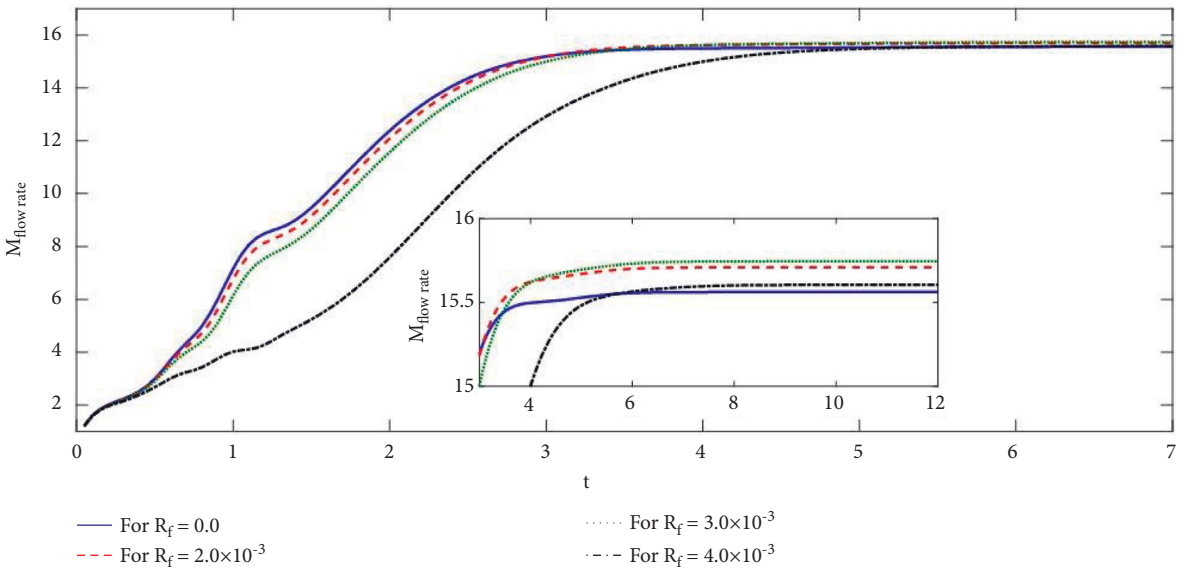

(b)

Figure 4: Continued.

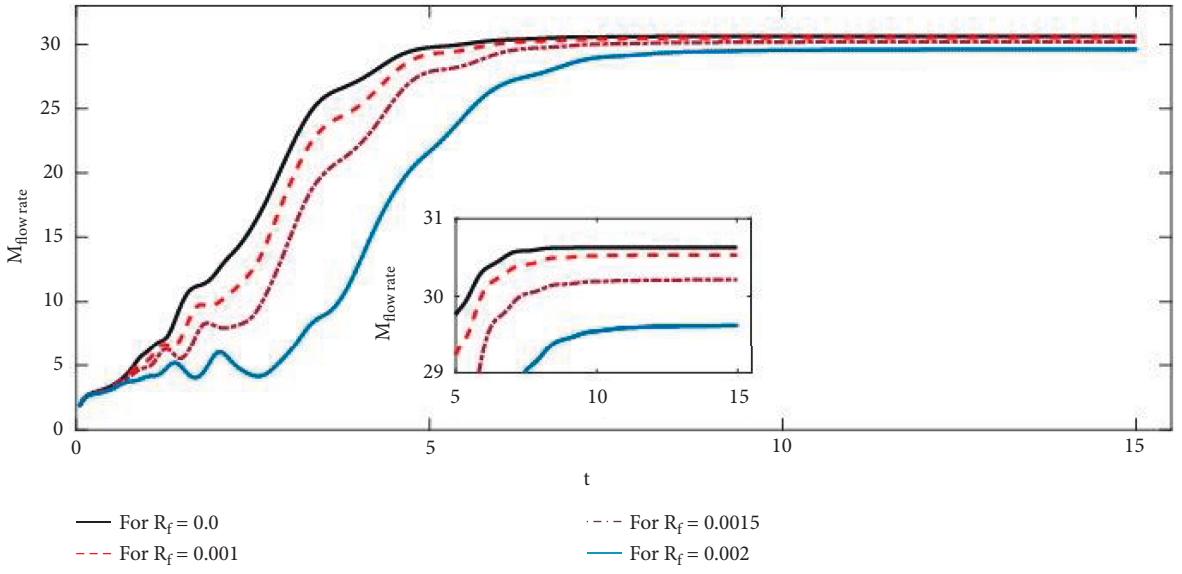

(c)

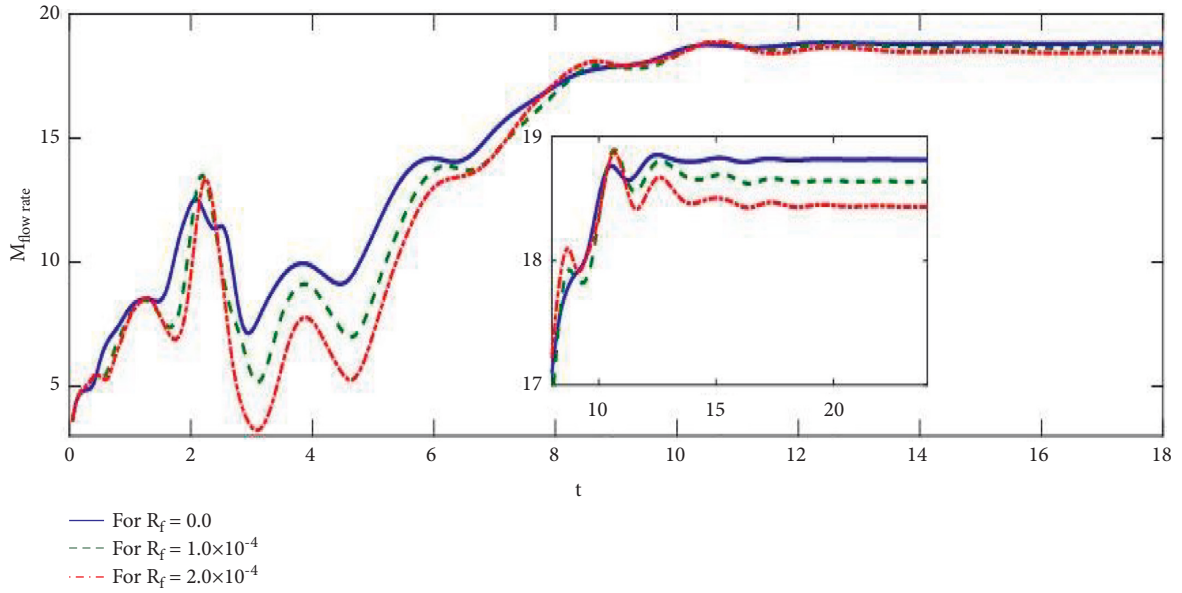

(d)

Figure 4: Mass flow rate with baffled length "L" = 0.25 for varying values of relaxation time 'R_t. (a) For Re = 500. (b) For Re = 1000. (c) For Re = 2000. (d) For Re = 5000.

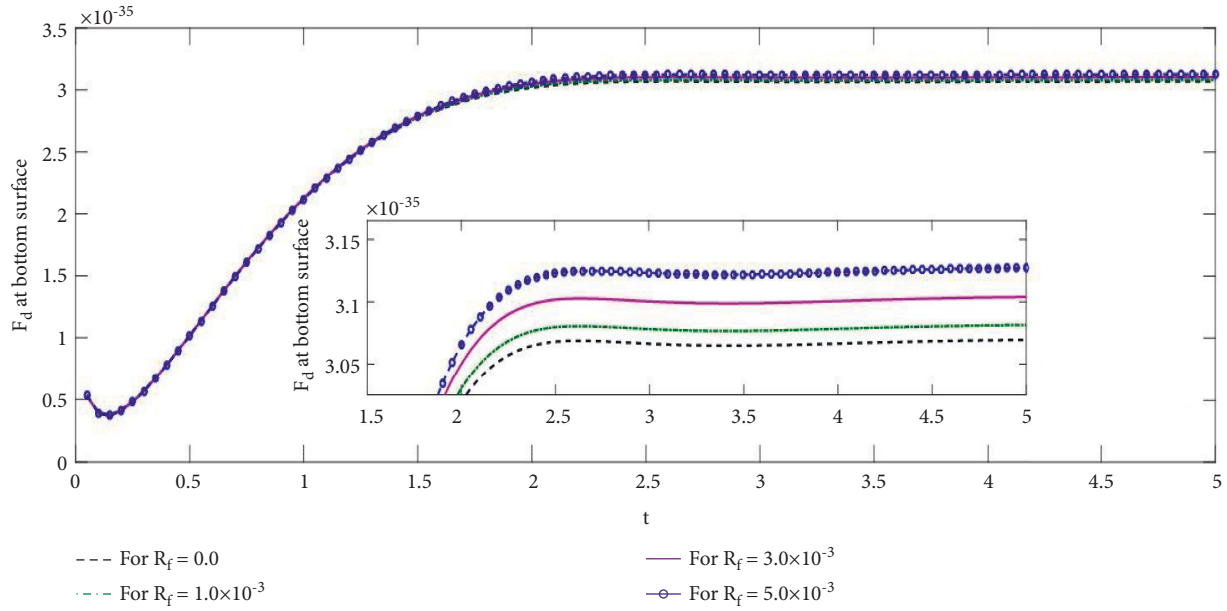

(a)

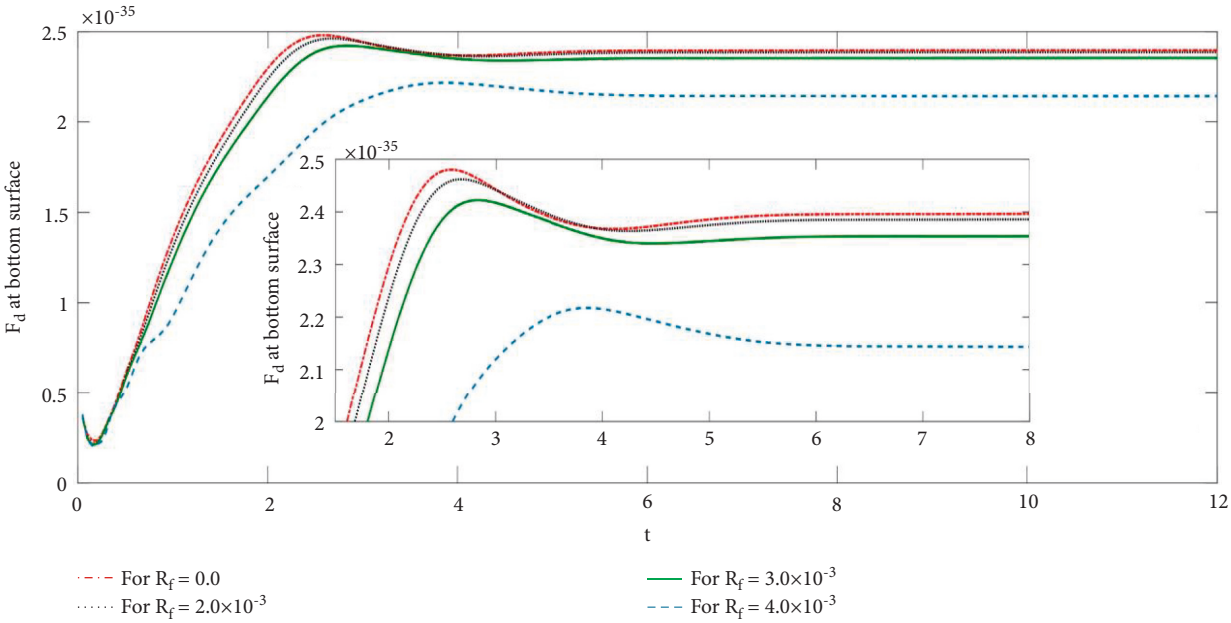

(b)

Figure 5: Continued.

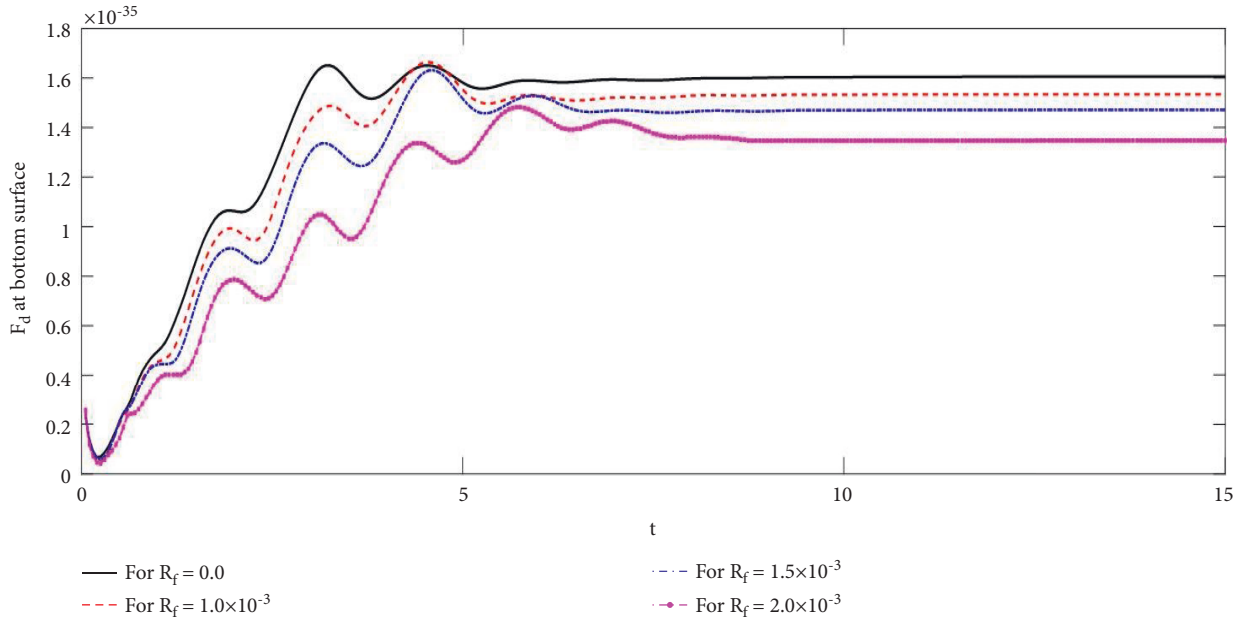

(c)

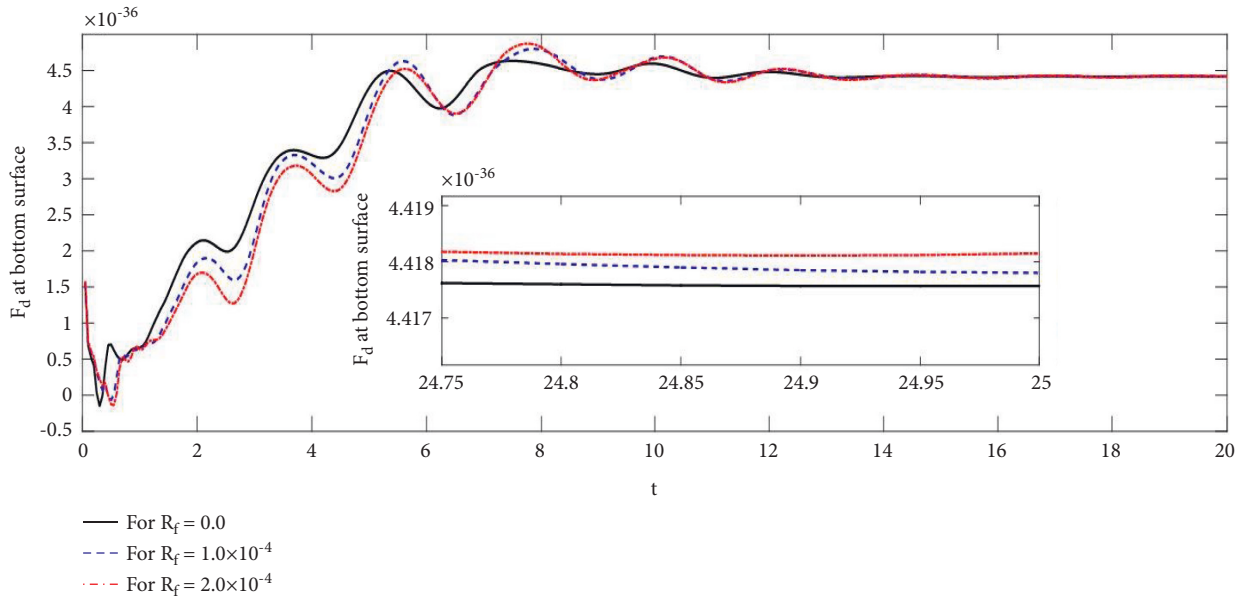

(d)

FIGURE 5: Drag force at the bottom surface with $L = 0.25$ and varying values of R_f. (a) For Re = 500, (b) for Re = 1000, (c) for Re = 2000, and (d) for Re = 5000.

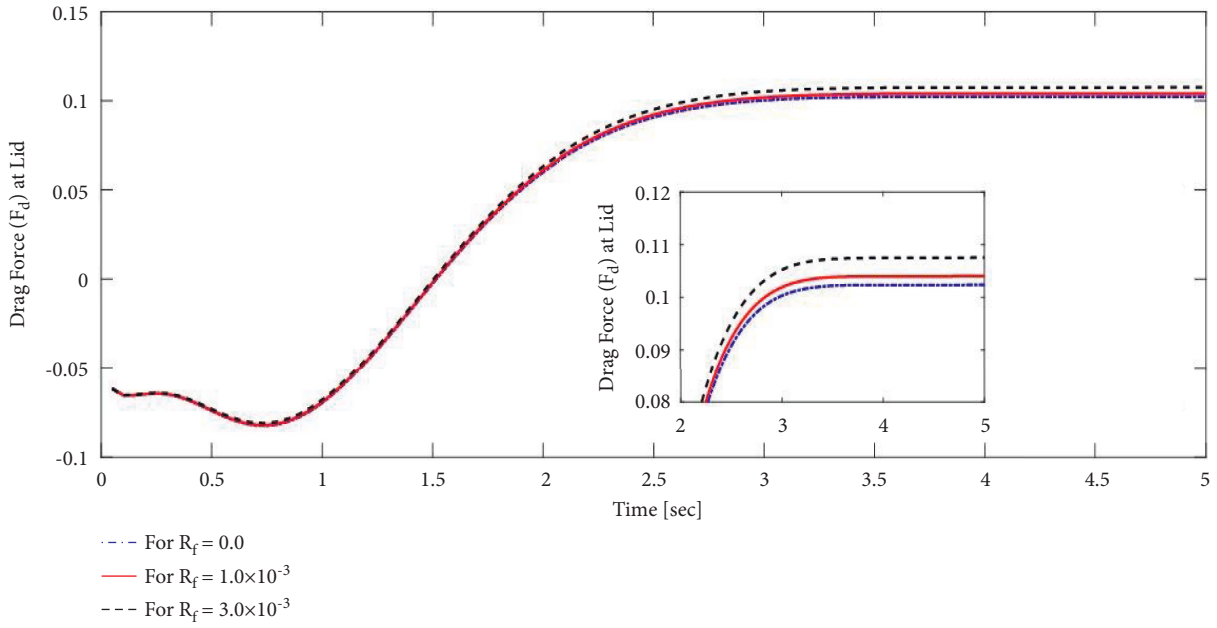

(a)

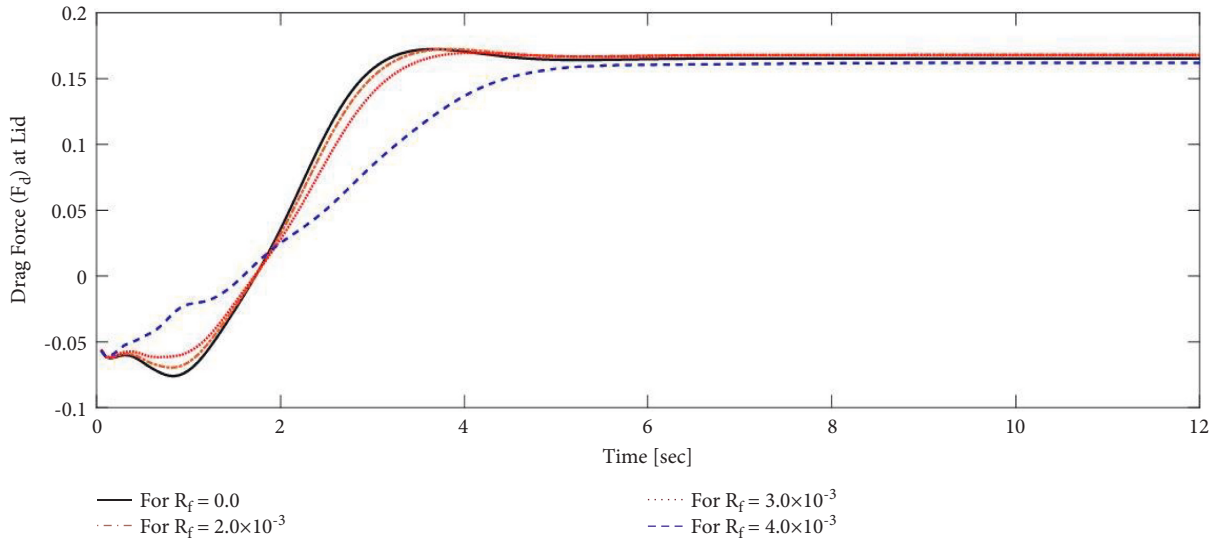

(b)

Figure 6: Continued.

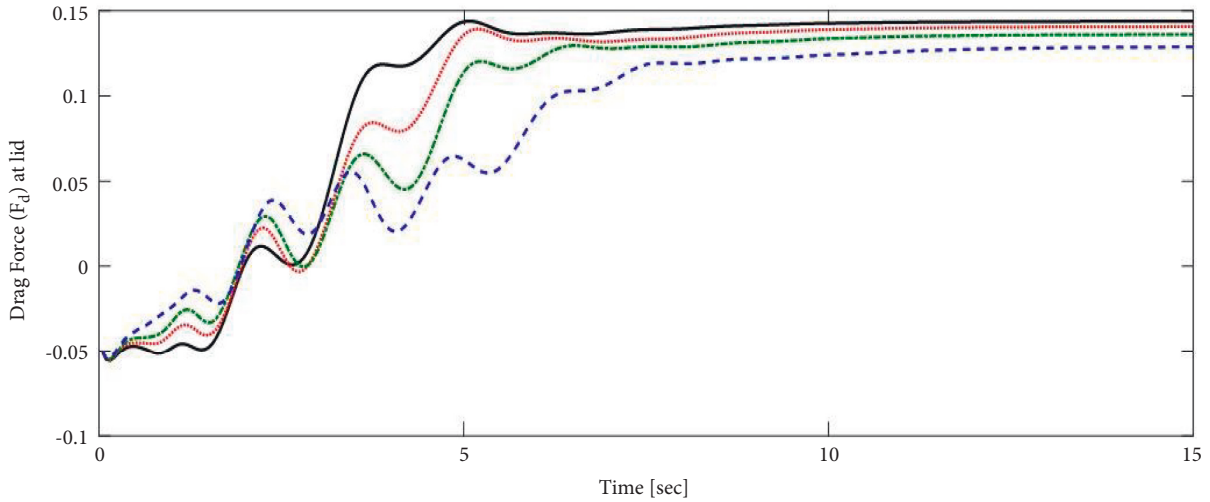

(c)

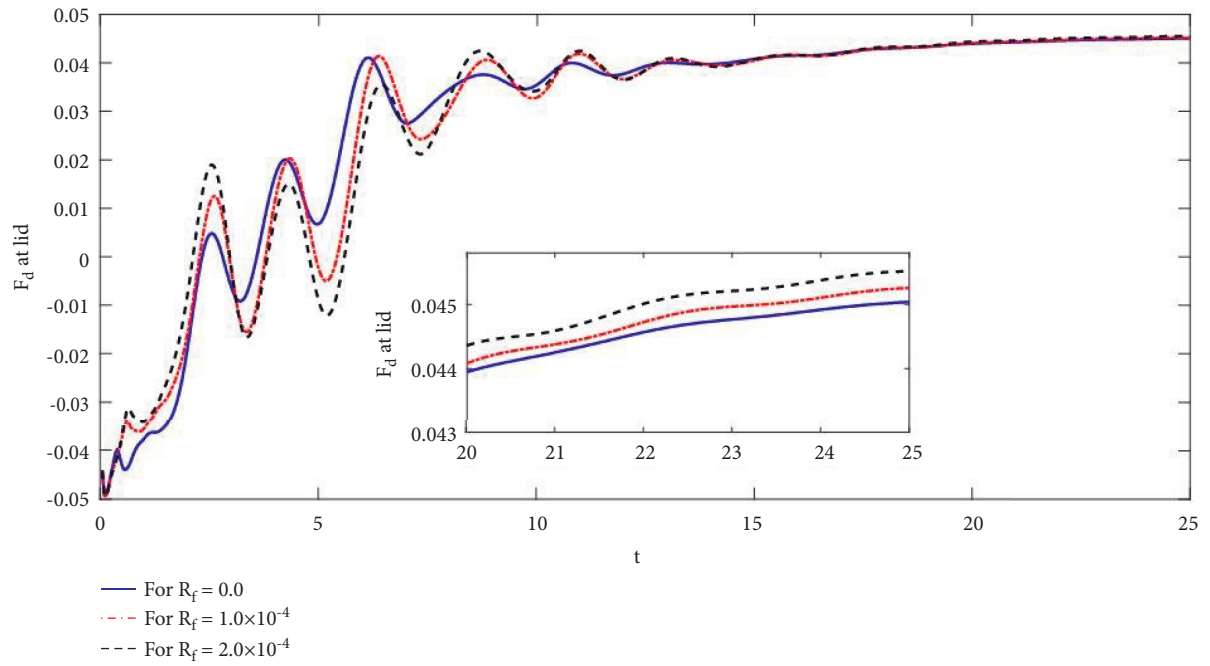

(d)

Figure 6: Drag force at the lid surface with $L = 0.25$ and varying values of R_f. (a) For Re = 500, (b) for Re = 1000, (c) for Re = 2000, and (d) for Re = 5000.

Table 1: Horizontal velocity component "u" for Re = 200 and Re = 1000 with varying values of the fluid relaxation parameter.

	Re = 200			Re = 1000			
R_f	0.0	5.0e-03	1.0e-02	0.0	2.0e-03	3.0e-03	4.0e-03
u(0.0;−0.4375)	−0.0137483	−0.01343	−0.01307	0.022477	0.022992	0.023175	0.0232
u(0.0;−0.375)	−0.030435	−0.0301	−0.02972	0.022345	0.023369	0.024148	0.026957
u(0.0;−0.3125)	−0.0526477	−0.05262	−0.05256	−0.00262	−0.00116	0.000669	0.009452
u(0.0;−0.25)	−0.0814902	−0.08209	−0.0827	−0.05809	−0.05666	−0.05352	−0.03549
u(0.0;−0.1875)	−0.116186	−0.11768	−0.11925	−0.1454	−0.14525	−0.14143	−0.11494
u(0.0;−0.125)	−0.152827	−0.15526	−0.15788	−0.24007	−0.24252	−0.24051	−0.21917
u(0.0;−0.0625)	−0.183365	−0.18637	−0.18965	−0.28028	−0.28396	−0.28567	−0.28997
u(0.0; 0.0)	−0.197098	−0.19985	−0.20293	−0.23835	−0.24078	−0.24431	−0.26833
u(0.0;0.0625)	−0.183887	−0.18551	−0.18744	−0.16095	−0.16228	−0.16535	−0.18881
u(0.0;0.125)	−0.140708	−0.14078	−0.1411	−0.08497	−0.08565	−0.08786	−0.10514
u(0.0;0.1875)	−0.0739784	−0.07263	−0.07142	−0.01022	−0.01031	−0.01177	−0.02398
u(0.0;0.25)	0.00552624	0.007896	0.010288	0.069609	0.070148	0.069384	0.061863
u(0.0;0.3125)	0.0919126	0.094687	0.097687	0.156061	0.157447	0.157462	0.155224
u(0.0;0.375)	0.208309	0.21068	0.213527	0.23781	0.240472	0.241445	0.245287
u(0.0;0.4375)	0.471098	0.472924	0.475312	0.318679	0.320737	0.321571	0.329919

Table 2: Vertical velocity component "v" for Re = 200 and Re = 1000 with varying values of the fluid relaxation parameter.

	Re = 200			Re = 1000			
Rf	0.0	5.0e-03	1.0e-02	0.0	2.0e-03	3.0e-03	4.0e-03
v(−0.4375;0.0625)	−0.0028463	−0.00295	−0.00304	−0.00894	−0.00892	−0.00883	−0.0085
v(−0.375;0.0625)	0.00278488	0.002681	0.002603	−0.00709	−0.00707	−0.00687	−0.00528
v(−0.3125;0.0625)	0.0223357	0.022341	0.022417	0.012148	0.012473	0.013114	0.017553
v(−0.25;0.0625)	0.11937	0.120209	0.121301	0.15859	0.15996	0.160095	0.15937
v(−0.1875;0.0625)	0.240211	0.243157	0.246468	0.269763	0.271332	0.269374	0.254121
v(−0.125;0.0625)	0.245026	0.248092	0.251353	0.275032	0.276508	0.274746	0.261233
v(−0.0625;0.0625)	0.211699	0.214401	0.217148	0.226727	0.226888	0.225338	0.215756
v(0.0; 0.0625)	0.159801	0.161952	0.164013	0.14581	0.145365	0.144234	0.137739
v(0.0625;0.0625)	0.0885403	0.089844	0.090932	0.063804	0.063391	0.062551	0.056993
v(0.125;0.0625)	−0.0018371	−0.00158	−0.00163	−0.01235	−0.01281	−0.01355	−0.01922
v(0.1875;0.0625)	−0.107099	−0.10807	−0.10939	−0.08679	−0.08746	−0.08826	−0.09491
v(0.25;0.0625)	−0.214806	−0.21728	−0.22007	−0.16888	−0.16964	−0.17084	−0.18173
v(0.3125;0.0625)	−0.29301	−0.29694	−0.30103	−0.27401	−0.27493	−0.27618	−0.28749
v(0.375;0.0625)	−0.288203	−0.29211	−0.29585	−0.3625	−0.36493	−0.36319	−0.34152
v(0.4375;0.0625)	−0.168197	−0.16994	−0.17139	−0.21667	−0.21569	−0.20769	−0.15334

Table 3: Variable of interest ϕ for Re = 200 and Re = 1000 with varying values of the fluid relaxation parameter.

		Re = 200		
R_f	0.0	5.0e-03	1.0e-02	
(ϕ)				
$\Psi_{\min}$	−2.30958e-04	−2.39755e-04	−2.48093e-04	
$\Psi_{\max}$	9.1456e-02	9.21415e-02	9.28754e-02	
M	2.67847	2.71165	2.7487	
F_{DL}	−2.5235e-02	−2.29625e-02	−2.0483e-02	
F_{DB}	2.77369e-35	2.82054e-35		
$u_{\min}$	−4.52796e-01	−4.26949e-01	−3.79307e-01	
$v_{\min}$		−7.42482e-01	−8.45826e-01	
$v_{\max}$		6.21795e-01	6.7349e-01	
		Re = 1000		
R_f	0.0	2.0e-03	3.0e-03	4.0e-03
(ϕ)				
$\Psi_{\min}$	−3.71524e-03	−3.91257e-03	−4.05054e-03	−4.64216e-03
$\Psi_{\max}$	8.14042e-02	8.17579e-02	8.16398e-02	8.08365e-02
M	1.55632e+01	1.57104e+01	1.57462e+01	1.56052e+01
F_{DL}	1.65313e-01	1.68016e-01	1.67988e-01	1.61894e-01
F_{DB}	2.39683e-35	2.38622e-35	2.35416e-35	2.14298e-35
$u_{\min}$	−6.10021e-01	−5.9926e-01	−5.66658e-01	−5.35703e-01
$v_{\min}$	−7.81665e-01	−8.6319e-01	−9.43754e-01	−1.17468e-00
$v_{\max}$	4.23152e-01	4.34828e-01	4.70203e-01	6.33143e-01

Table 4: Kinetic energy values for varying values of the fluid relaxation parameter.

Lx	Rf	K. E.				
		Re = 200	Re = 500	Re = 1000	Re = 2000	Re = 5000
0.25	0.0	2.86122e-02	2.65885e-02	2.39189e-02	1.92665e-02	1.07067e-02
	1.0e-04	2.86193e-02	—	—	—	1.07138e-02
	2.0e-04	2.86264e-02	—	—	—	1.07223e-02
	1.0e-03	2.86837e-02	2.67108e-02	—	1.96793e-02	—
	1.5e-03	—	—	—	2.01988e-02	—
	2.0e-03	—	—	2.41302e-02	2.05156e-02	—
	3.0e-03	2.88331e-02	2.69734e-02	2.40805e-02	—	—
	4.0e-03	—	—	2.4216e-02	—	—
	5.0e-03	2.89889e-02	2.73547e-02	—	—	—
	1.0e-02	2.94589e-02	—	—	—	—

5. Conclusions

This study aims to understand the rheology of complex liquids important to model different physical problems arising in a wide range of industrial applications. In this respect, a fluid relaxation time nonlinear PDE model is presented and numerically investigated. In particular, the effect of fluid relaxation time on the characteristics of viscoelastic flow dynamics is examined. As a model test problem, a two-dimensional lid-driven baffled cavity is chosen for the analysis. Computations are performed using characteristic Galerkin finite elements, and a developed code is implemented through FreeFem++. Different features of the flow characteristics are computed and presented through graphs and tables. Some of the main findings are summarized in the following points:

(i) In the laminar regime of flow, the relaxation time raises the mass flow rate, whereas in the transitional flow regime, the relaxation time drops the mass flow rate.

(ii) The kinetic energy of the system of particles in flow gets increased by increasing the fluid relaxation time. This result is in accordance with the observations of Josef et al. [17] where an increase in the swimmer speed was observed by increasing the fluid relaxation time.

(iii) The drag force at the bottom surface decreases as relaxation time is increased in both the laminar and transitional regimes.

(iv) The drag force shows a nonmonotone behavior in the regime of low Reynolds numbers at the lid surface, and it decreases by increasing the relaxation time when flow gets near the transitional regime.

(v) The minimum stream value $\psi_{\min}$ decreases with the increasing value of the relaxation time.

(vi) The maximum stream value $\psi_{\max}$ ψmax increases monotonically with increasing relaxation time in case of Re = 200, whereas this relation becomes nonmonotone in the case of large Re = 1000. Moreover, in the case of Re = 1000 and chosen relaxation times, the maximum value of $\psi_{\max}$ gets $R_f = 2.0 \times 103$.

Data Availability

No data were used to support this study.

Conflicts of Interest

The authors declare that there are no conflicts of interest regarding the publication of this paper.

References

[1] M. Zhang, E. Yang, J. Zeng, J. Ji, F. Tian, and L. Li, "Numerical study on oblique stretching of viscoelastic polymer film," *Journal of Non-newtonian Fluid Mechanics*, vol. 295, Article ID 104597, 2021.

[2] D. Tang, F. H. Marchesini, L. Cardon, and D. R. D'hooge, "Three-dimensional flow simulations for polymer extrudate swell out of slit dies from low to high aspect ratios," *Physics of Fluids*, vol. 31, Article ID 93103, 2019.

[3] C. Czibula, T. Seidlhofer, C. Ganser, U. Hirn, and C. Teichert, "Longitudinal and transverse low frequency viscoelastic characterization of wood pulp fibers at different relative humidity," *Materialia*, vol. 16, Article ID 101094, 2021.

[4] B. Derakhshandeh, R. J. Kerekes, S. G. Hatzikiriakos, and C. P. J. Bennington, "Rheology of pulp fibre suspensions: a critical review," *Chemical Engineering Science*, vol. 66, no. 15, pp. 3460–3470, 2011.

[5] S. Stieger, E. Mitsoulis, M. Kämpfe et al., "On the influence of viscoelastic modeling in fluid flow simulations of gum acrylonitrile butadiene rubber," *Polymers*, vol. 13, no. 14, Article ID 2323, 2021.

[6] M. s. Kassim and S. A. Sarow, "Flows of viscous fluids in food processing industries: a review," *IOP Conference Series: Materials Science and Engineering*, vol. 870, no. 1, Article ID 012032, 2020.

[7] F.-J. Rubio-Hernández, "Rheological behavior of fresh cement pastes," *Fluid*, vol. 3, no. 4, p. 106, 2018.

[8] M. Pelton, D. Chakraborty, E. Malachosky, P. Guyot-Sionnest, and J. E. Sader, "Viscoelastic flows in simple liquids generated by vibrating nanostructures," *Physical Review Letters*, vol. 111, no. 24, Article ID 244502, 2013.

[9] Z. Chen and D. Ceballos-Francisco, "The alleviation of skin wound-induced intestinal barrier dysfunction via modulation of TLR signalling using arginine in gilthead seabream (*Sparus aurata* L)," *Fish & Shellfish Immunology*, vol. 107, no. Pt B, pp. 519–528, 2020.

[10] G. Li, E. Lauga, and A. M. Ardekani, "Microswimming in viscoelastic fluids," *Journal of Non-newtonian Fluid Mechanics*, vol. 297, Article ID 104655, 2021.

[11] B. Qin, "Flow behavior and instabilities in viscoelastic fluids: physical and biological systems," *Publicly Accessible Penn Dissertations*, University of Pennsylvania, no. 3174, Philadelphia, PA, USA, 2018.

[12] C. Yuan, H.-N. Zhang, Y. K. Li, X.-B. Li, J. Wu, and F.-C. Li, "Nonlinear effects of viscoelastic fluid flows and applications in microfluidics: a review," *Proceedings of the Institution of Mechanical Engineers - Part C: Journal of Mechanical Engineering Science*, vol. 234, no. 22, pp. 4390–4414, 2020.

[13] L. Zhu, E. Lauga, and L. Brandt, "Self-propulsion in viscoelastic fluids: pushers vs. pullers," *Physics of Fluids*, vol. 24, no. 5, Article ID 051902, 2012.

[14] B. Sebastian and P. S. Dittrich, "Microfluidics to mimic blood flow in health and disease," *Annual Review of Fluid Mechanics*, vol. 50, no. 1, pp. 483–504, 2018.

[15] S. S. Suarez and A. A. Pacey, "Sperm transport in the female reproductive tract," *Human Reproduction Update*, vol. 12, no. 1, pp. 23–37, 2006.

[16] S. J. Haward, K. Toda-Peters, and A. Q. Shen, "Steady viscoelastic flow around high-aspect-ratio, low-blockage-ratio microfluidic cylinders," *Journal of Non-newtonian Fluid Mechanics*, vol. 254, no. 13, pp. 23–35, 2018.

[17] S. Gulati, S. J. Muller, and D. Liepmann, "Direct measurements of viscoelastic flows of DNA in a 2:1 abrupt planar micro-contraction," *Journal of Non-newtonian Fluid Mechanics*, vol. 155, no. 1-2, pp. 51–66, 2008.

[18] R. E. Goldstein, "Green algae as model organisms for biological fluid dynamics," *Annual Review of Fluid Mechanics*, vol. 47, no. 1, pp. 343–375, 2015.

[19] K. T. Kotz, W. Xiao, C. Miller-Graziano et al., "Clinical microfluidics for neutrophil genomics and proteomics," *Nature Medicine*, vol. 16, no. 9, pp. 1042–1047, 2010.

[20] P. Liu, H. Liu, L. Semenec et al., "Length-based separation of Bacillus subtilis bacterial populations by viscoelastic microfluidics," *Microsystems & Nanoengineering*, vol. 8, no. 1, p. 7, 2022.

[21] M. A. Alves, P. J. Oliveira, and F. T. Pinho, "Numerical methods for viscoelastic fluid flows," *Annual Review of Fluid Mechanics*, vol. 53, no. 1, pp. 509–541, 2021.

[22] B. Mahapatra and A. Bandopadhyay, "Electroosmosis of a viscoelastic fluid over non-uniformly charged surfaces: effect of fluid relaxation and retardation time," *Physics of Fluids*, vol. 32, no. 3, Article ID 032005, 2020.

[23] D. Dey, "Viscoelastic fluid flow through an annulus with relaxation, retardation effects and external heat source/sink," *Alexandria Engineering Journal*, vol. 57, no. 2, pp. 995–1001, 2018.

[24] I. M. Eldesoky, R. M. Abumandour, and E. T. Abdelwahab, "Analysis for various effects of relaxation time and wall properties on compressible maxwellian peristaltic slip flow," *Zeitschrift für Naturforschung A*, vol. 74, no. 4, pp. 317–331, 2019.

[25] J. Teran, L. Fauci, and M. Shelley, "Viscoelastic fluid response can increase the speed and efficiency of a free swimmer," *Physical Review Letters*, vol. 104, no. 3, Article ID 038101, 2010.

[26] F. Hecht, "New development in FreeFem++," *Journal of Numerical Mathematics*, vol. 20, no. 3-4, pp. 251–265, 2012.

[27] R. B. Bird, R. C. Armstrong, and O. Hassager, *Dynamics of Polymeric Liquids: Fluid Mechanics*, Wiley, New York City, NY, USA, 1987.

[28] O. Pironneau, J. Liou, and T. Tezduyar, "Characteristic-Galerkin and Galerkin/least-squares space-time formulations for the advection-diffusion equation with time-dependent domains," *Computer Methods in Applied Mechanics and Engineering*, vol. 100, no. 1, pp. 117–141, 1992.

[29] J. Zilz, C. Schäfer, C. Wagner, R. J. Poole, M. A. Alves, and A. Lindner, "Serpentine channels: micro-rheometers for fluid relaxation times," *Lab on a Chip*, vol. 14, no. 2, pp. 351–358, 2014.